Strain Controlled Spin and Charge Pumping in Graphene Devices via Spin-orbit Coupled Barriers

RAMIN MOHAMMADKHANI[1] , BABAK ABDOLLAHIPOUR[2] and MOHAMMAD ALIDOUST[3,4]

[1] *Department of Physics, Faculty of Science, University of Zanjan, Zanjan 45371-38791, Iran*
[2] *Faculty of Physics, University of Tabriz, Tabriz 51666-16471, Iran*
[3] *Department of Physics, University of Basel, Klingelbergstrasse 82, CH-4056 Basel, Switzerland*
[4] *Department of Physics, Faculty of Sciences, University of Isfahan, Hezar Jerib Avenue, Isfahan 81746-73441, Iran*

arXiv:1702.00246v1 [cond-mat.mes-hall] 1 Feb 2017

PACS nn.mm.xx – 73.63.-b
PACS nn.mm.xx – 72.80.Vp
PACS nn.mm.xx – 72.25.-b

Abstract – We theoretically propose a graphene-based adiabatic quantum pump with intrinsic spin-orbit coupling (SOC) subject to strain where two time-dependent extrinsic spin-orbit coupled barriers drive spin and charge currents. We study three differing operation modes where i) location, ii) chemical potential, and iii) SOC of the two barriers oscillate periodically and out of phase around their equilibrium states. Our results demonstrate that the amplitude of adiabatically pumped currents highly depends on the considered operation mode. We find that such a device operates with highest efficiency and in a broader range of parameters where the barriers' chemical potential drives the quantum pump. Our results also reveal that by introducing strain to the system, one can suppress or enhance the charge and spin currents separately, depending on strain direction.

Spintronics is an emerging filed which has aimed at exploiting the spin degree of freedom to construct faster and high performance low-power nanoscale devices [1]. The discovery of isolated graphene monolayer [2, 3], a single layer of Carbon atoms, with unique electrical, optical and thermal properties has triggered numerous efforts to achieve graphene-based nanoscale devices [5–8]. The massless Dirac fermions in ballistic graphene can reflect chirality and linear dispersion relation of graphene around the Dirac points; two inequivalent corners of the first Brillouin zone [4]. Also, the long spin relaxation time of the Dirac fermions in graphene monolayers due to a small intrinsic spin-orbit coupling (SOC) which originates from the intra-atomic spin-orbit coupling of the Carbon atoms has made it an exceptional candidate to the spintronics devices [7].

Quite recently, it was experimentally demonstrated that a strong Rashba SOC $\sim$ 17 meV can be induced into graphene monolayers by means of proximity to a semiconducting tungsten disulphide substrate [8]. This finding is highly appealing in terms of generation and manipulation of spin currents in more controllable platforms. The intrinsic SOC that can be caused by the crystalline potential associated with the band structure respects all the lattice symmetries in graphene and results in a small energy gap at the Dirac points. The extrinsic or Rashba SOC, however, results from the lack of inversion symmetry due to perpendicular electric fields, substrate effects, chemical doping, or curvature of graphene corrugations and can be responsible for inducing a spin polarization in graphene. [9, 10] The influences of intrinsic and Rashba SOCs on the transport properties of graphene monolayer systems have extensively been studied in the recent years [5, 6, 11–14]. For instance, it was shown that spin polarization induced by a charge current can reside in the graphene plane and perpendicular to the electric field while its sign changes by varying the Fermi level through an external gate voltage [11]. Also, it was theoretically found that the interplay of massive electrons with SOC or strain in a graphene layer can result in a spin-valley filter [13, 15].

Spin and charge quantum pumpings are striking topics in the context of quantum transport through nanostructures. The quantum nature of these effects arises from the geometric (Berry) phases and quantum interference effects [16]. An adiabatically pumped current requires, at least, two parameters of system vary periodically and out of phase in time [17]. The adiabaticity is achieved when the characteristic time of the variations is much smaller than the dwell time of carriers. In this base, several proposals for charge pumping through graphene junctions were introduced during the past years [18–26].

Motivated by the recent researches on time-dependent graphene systems [18–26] and experimentally achieved graphene layers with strong extrinsic spin-orbit couplings [8,

10, 27], in this paper we propose a novel device to generate controllable charge and spin pumped currents without resorting to any externally imposed field. This device consists of a graphene monolayer with length $2L$ and width W under strain with intrinsic spin-orbit coupling and the pumped currents are driven by two extrinsic spin-orbit coupled barriers induced by a substrate [8].

We assume that the chemical potential/ location or SOC of the barriers can be time-dependent and periodically oscillate out of phase. Our results reveal that the quantum pump operates with highest efficiency where the barriers chemical potential drives the currents. It is shown that, in the latter case, the currents' amplitude is more pronounced and the quantum pump operates in a broader range of the system parameters. We also uncover how an in-plane strain in the graphene layer alters and controls the spin and change currents simultaneously. Our results demonstrate that a weak strain applied to the graphene plane can enhance the spin current and suppress the charge current simultaneously, depending on the direction of strain.

The quasiparticles at low energies in a monolayer of graphene under tension and in the presence of intrinsic and extrinsic SOCs (ISO and ESO) are governed by the following Hamiltonian [9, 12]:

$$\begin{aligned}&\mathcal{H}=\mathcal{H}_0+\mathcal{H}_{\rm ISO}+\mathcal{H}_{\rm ESO};\\&\mathcal{H}_0=v_xp_xs_0\sigma_x+v_yp_ys_0\sigma_y+\mu(x)s_0\sigma_0,\\&\mathcal{H}_{\rm ISO}=\beta s_z\sigma_z,\quad \mathcal{H}_{\rm ESO}=\alpha[s_y\sigma_x-s_x\sigma_y].\end{aligned}\tag{1}$$

Here, $\mu(x)$ is a tuneable chemical potential which can be controlled by an external gate voltage. β and α are the strength of intrinsic and extrinsic SOCs, respectively. σ_0 and s_0 denote 2×2 unitary matrices, σ_i and $s_i (i=x,y,z)$ are the Pauli matrices in the pseudospin and the real spin subspaces, respectively. The proposed quantum pump is schematically depicted in Fig. 1. There are two electrode regions where carriers' density can be externally controlled. The entire of graphene layer is assumed intrinsically spin-orbit coupled. We focus on strains applied in two distinct crystallographic directions: zig-zag (Z) and armchair (A) as shown in Fig. 1. In order to study the influences of strain on the characteristics of system transport, we adopt a model introduced in Ref. [28] and expand tight-binding result for the band structure with arbitrary hopping energies $t_{1,2,3}$ around the new Dirac point $\mathbf{K}_D=(\cos^{-1}(-1/2\eta)/\sqrt{3}a_x,0)$, namely, $E_k=\pm|\sum_{i=1}^{3}t_ie^{-i\vec{k}.\vec{\delta}_i}|$ [29, 30]. As shown in Fig. 1, $\vec{\delta}_i$ are displacement vectors between two nearest neighbor Carbon atoms. We assume $t_1=t_2=\tilde{\epsilon}$ and $t_3=\epsilon$ in our calculations and set η equal to ratio $\tilde{\epsilon}/\epsilon$. The quasiparticles' velocities are given by $v_x=2\tilde{\epsilon}a_x\sin(\cos^{-1}(-1/2\eta))/\hbar$ and $v_y=3\epsilon a_y/2\hbar$ [29, 30]. The hoping energies are given by $t_i=\epsilon_0e^{-3.37(|\vec{\delta}_i|)/c_0-1}$, where $c_0=0.142\mathring{A}$ and ϵ_0 are the distance of two Carbon atoms and hoping energy in the undeformed graphene layer, respectively. The displacement vectors under the Z-strain leads to $\vec{\delta}_1=a_x\sqrt{3}\hat{x}-a_y\hat{y}$, $\vec{\delta}_2=-a_x\sqrt{3}\hat{x}-a_y\hat{y}$, $\vec{\delta}_3=2a_y\hat{y}$ while for the armchair (A-strain), $\vec{\delta}_1=a_y\sqrt{3}\hat{x}-a_x\hat{y}$, $\vec{\delta}_2=-a_y\sqrt{3}\hat{x}-a_x\hat{y}$, $\vec{\delta}_3=2a_x\hat{y}$. Here $a_x=(1+s)c_0/2$ and $a_y=c_0(1-ps)/2$ with $p=0.165$ which is the Poisson's ratio for graphite and s represents the strength of applied tension. The *maximum* tension strength considered throughout this paper can be less than the gap threshold value, i.e. $s\leq 0.23\sim 20\%$ predicted theoretically (see Ref. [28, 31]). The experimental evidence for maximum strain exerted on graphene without change in its band structure is less than $\sim 15\%$ [32]. Nonetheless, we emphasize that a maximum of $\sim 15\%$ does not affect the main conclusions of this paper. We have used the generalized Weyl-Hamiltonian which is in a very good agreements with the *ab initio* calculations. If we diagonalize the total Dirac Hamiltonian $\mathcal{H}$ given by Eq. (1), we arrive at the following spinors in each region of the system represented by $\gamma=1,2,3,4,5$ (see Fig. 1)

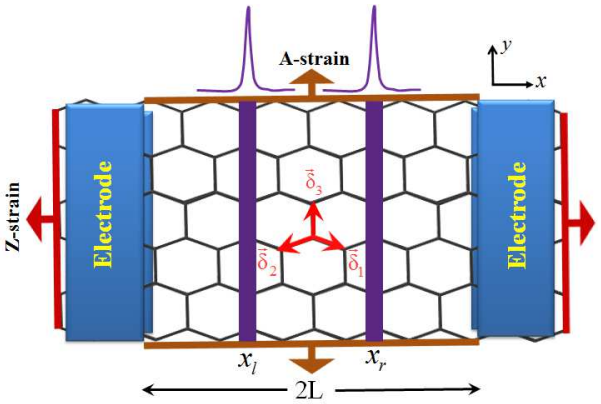

Fig. 1: Schematic of the strained graphene quantum pump proposed in this paper. Two time-dependent barriers located at x_l and x_r pump spin and charge currents across the system which are modeled by the Dirac delta function. The system contains 5 regions (γ) from left to right: $(\gamma)=(1),(5)$ are electrode regions and $(\gamma)=(2),(3),(4)$ regions are the ISO coupled graphene segments separated by the vibrating barriers. We assume that the strain imposed can be either in A- or Z-direction and label them by A-strain/Z-strain.

$$\psi_+^{\pm}(x_\gamma,\varepsilon_n)=(1,\pm\zeta_{n,+}^{\gamma,\pm},0,0)e^{i(\pm\kappa_n^\gamma x_\gamma+q_ny)}\tag{2}$$

$$\psi_-^{\pm}(x_\gamma,\varepsilon_n)=(0,0,1,\pm\zeta_{n,-}^{\gamma,\pm})e^{i(\pm\kappa_n^\gamma x_\gamma+q_ny)}\tag{3}$$

$$\kappa_n^\gamma=\Big(\frac{\varepsilon_{F\gamma}^2-\beta_\gamma^2-\hbar^2v_{y\gamma}^2q_n^2}{\hbar^2v_{x\gamma}^2}\Big)^{1/2},\ \zeta_{n,\sigma}^{\gamma,\pm}=\frac{v_{x\gamma}\kappa_n^\gamma\pm iv_{y\gamma}q_n}{\sigma\beta_\gamma+\varepsilon_{F\gamma}}$$

where $\sigma=\pm$, $\varepsilon_{F\gamma}$ is the quasiparticles' energy measured from the chemical potential level, and q_n stands for the transverse component of the wave vector which is conserved in different γ regions. The junction is assumed sufficiently wide, $W\gg L$, which allows for replacing $\sum_{q_n}$ by $\int dq$ in our calculations. For numerical purposes, we define the total wave vector $\mathcal{K}_n^\gamma$,

i.e. $\kappa_n^\gamma = \mathcal{K}_n^\gamma \cos\theta_{n,\gamma}$ and $q_n = \mathcal{K}_n^\gamma \sin\theta_{n,\gamma}$, as follows:

$$\hbar\mathcal{K}_n^\gamma = \Big(\frac{\varepsilon_{F\gamma}^2 - \beta_\gamma^2}{v_{x\gamma}^2\cos^2\theta_{n,\gamma} + v_{y\gamma}^2\sin^2\theta_{n,\gamma}}\Big)^{1/2}, \tag{4a}$$

$$\zeta_{n,\sigma}^{\gamma,\pm} = \sqrt{\frac{\varepsilon_{F\gamma} - \sigma\beta_\gamma}{\varepsilon_{F\gamma} + \sigma\beta_\gamma}}\,\frac{v_{x\gamma}\cos\theta_{n,\gamma} \pm i v_{y\gamma}\sin\theta_{n,\gamma}}{\sqrt{v_{x\gamma}^2\cos^2\theta_{n,\gamma} + v_{y\gamma}^2\sin^2\theta_{n,\gamma}}}, \tag{4b}$$

$$\theta_{n,\gamma} = \arcsin\Big[\frac{\hbar^2 q_n^2 v_{x\gamma}^2}{\varepsilon_{F\gamma}^2 - \beta_\gamma^2 + (v_{x\gamma}^2 - v_{y\gamma}^2)q_n^2}\Big]^{1/2}. \tag{4c}$$

To model the vibrating barriers shown in Fig. 1, we assume that experimentally tuneable parameters at the barriers are i) the chemical potentials $\mu_{l,r}$ and ii) the ESOC $\alpha_{l,r}$ in addition to iii) their locations $x_{l,r}$. The first mode, i, of the pumping can be realized by tuning the potential of underlying gats. To experimentally realize the two other modes one may construct the barriers through two flexible cantilevers with vertical and horizontal oscillations around their equilibrium locations on top of the graphene sheet, respectively. The total wave function of a particle Ψ passing through the barriers experiences the following transformation $\mathcal{T}_{l,r}$ at the left (l) and right (r) barriers namely, $\Psi^{\mathcal{R}} = \mathcal{T}_{l,r}\Psi^{\mathcal{L}}$ in which

$$\mathcal{T}_{l,r} = \frac{2i\hbar v_x^{\mathcal{L}} s_0\sigma_x + \mu_{l,r}s_0\sigma_0 + \alpha_{l,r}(s_y\sigma_x - s_x\sigma_y)}{2i\hbar v_x^{\mathcal{R}} s_0\sigma_x - \mu_{l,r}s_0\sigma_0 - \alpha_{l,r}(s_y\sigma_x - s_x\sigma_y)}. \tag{5}$$

The transformations $\mathcal{T}_{l,r}$ are derived by integrating the Dirac Hamiltonian Eq. (1) over the x-direction in close vicinities of the barriers and modeling the vibrating barriers through spatial Dirac deltas. [23, 33]. $v_x^{\mathcal{L}}$ and $v_x^{\mathcal{R}}$ show the velocity of particles at the left ($\mathcal{L}$) and right ($\mathcal{R}$) sides of the barriers. The charge and spin currents pumped by $\mathcal{X}_{l,r}$: two periodic and out of phase oscillating parameters at the barriers (and within the bilinear response regime where $\delta\mathcal{X}_{l,r} \ll \mathcal{X}_{l,r}$) can be expressed by [17, 23]:

$$I^{\mathcal{X}}_{\text{charge}}(I^{\mathcal{X}}_{\text{spin}}) = N_m I_0 \sum_{\sigma=\pm}\int_{-\infty}^{+\infty}\frac{dq}{\mathcal{K}_F}(\sigma)\text{Im}\Big\{\frac{\partial\mathfrak{R}_\sigma}{\partial\mathcal{X}_l}\frac{\partial\mathfrak{R}_\sigma^*}{\partial\mathcal{X}_r} + \frac{\partial\mathfrak{T}_\sigma}{\partial\mathcal{X}_l}\frac{\partial\mathfrak{T}_\sigma^*}{\partial\mathcal{X}_r}\Big\}, \tag{6}$$

in which the pumping parameters oscillate around equilibrium values $\mathcal{X}_{l,r}(0)$ and are given by $\mathcal{X}_{l,r}(t) = \mathcal{X}_{l,r}(0) + \delta\mathcal{X}_{l,r}\cos(\Omega t + \varphi_{l,r})$. To reside in the adiabatic regime, the pumping frequency should be of terahertz range, i.e., $\Omega/2\pi \sim$1 THz [18]. The spin-dependent reflection and transition coefficients are denoted by $\mathfrak{R}_\sigma$ and $\mathfrak{T}_\sigma$, respectively. Here $I_0 = 0.5\pi^{-1}\Omega e\delta\mathcal{X}_l\delta\mathcal{X}_r\sin\varphi$ in which $\varphi = \varphi_r - \varphi_l$ is the phase difference of two oscillating parameters. In what follows, we normalize the currents by $I_0 N_m$, and thus define $I_c^{\mathcal{X}} = I^{\mathcal{X}}_{\text{charge}}/I_0 N_m$, $I_s^{\mathcal{X}} = I^{\mathcal{X}}_{\text{spin}}/I_0 N_m$ where N_m is the number of available modes at the fermi level.

Figure 2 exhibits the charge and spin currents adiabatically pumped where the strength of ESOCs at the right and left barriers serve as the pumping parameters with the same equilibrium

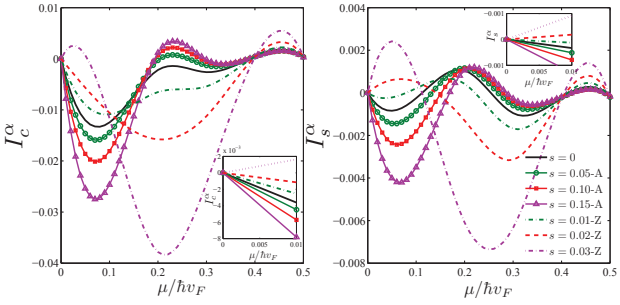

Fig. 2: Adiabatically pumped charge and spin currents: I_c^α and I_s^α as a function of chemical potential at the left and right barriers $\mu_l = \mu_r = \mu$. The time dependent parameters are the strength of ESOCs at the left and right barriers ($\alpha_{l,r}$) and their equilibrium strengths are set fixed at $\alpha_l = \alpha_r = 3.5\hbar v_F$. Two kinds of strain ($A$ and Z) are considered at three differing values of strain s: A-strain, $s = 0.05, 0.10, 0.15$ and Z-strain, $s = 0.01, 0.02, 0.03$.

values $\alpha_l = \alpha_r = \alpha$ and $\mu_l = \mu_r = \mu$. The parameters of the barriers are set at $\alpha_{l,r} = 3.5\hbar v_F$, $x_l = 0.0$, $x_r = 0.5L$, while the chemical potential of regions $\gamma = 2, 3, 4$ are considered fixed at $\mu_{2,3,4} = 0.5\hbar v_F$. The intrinsic spin-orbit coupling is assumed constant throughout the graphene layer $\beta = 0.02\hbar v_F$ which is equivalent to ≈ 0.05meV and the extrinsic SO is about $\alpha \approx 9.0$meV [10,27] . The pumped currents are plotted against the doping level of the barriers i.e. $\mu_{r,l}$ normalized by $\hbar v_F$. Here $2L$ is the junction length (see Fig. 1) and v_F is the velocity of Dirac fermions at the fermi level in an undeformed graphene sheet i.e. $v_x = v_y = v_F$. The left and right panels show the charge and spin currents (I^α_{charge} and I^α_{spin} normalized by $N_m I_0$), respectively. The inset panels are close-ups of the currents where the barriers' chemical potential is restricted to $0 < \mu < 0.01\hbar v_F$. The solid black lines exhibit the currents where no strain is exerted to the system ($s = 0$), in contrast to the other curves which show the effect of the in plane strain imposed to the graphene layer. We have considered both armchair and zig-zag strains as sketched in Fig. 1. To have similar magnitudes for the pumped currents, we set $s = 0.05, 0.10, 0.15$ for the strength of the A-strain while $s = 0.01, 0.02, 0.03$ for the Z-strain. The values of s considered here ensure that the strain is enough weak $s < 20\%$, so that no gap opens in the particles' energy spectrum [29, 30, 34, 35]. As seen, the pumped charge current is one order of magnitude greater than the spin current. Figure 2 illustrates how the charge and spin currents can be manipulated through applying strain in different directions to the device. The spin current can change sign while the charge current direction remains intact upon moving from $s = 0.01$-Z to 0.02-Z at $\mu \sim 0.05\hbar v_F$. By increasing the tension the overall amplitudes of the pumped currents for both A- and Z-directions enhance. Also, the inset panels reveal that the charge and spin currents are zero at $\mu = 0$ independent of the strain direction applied.

Figure 3 shows the adiabatically pumped charge and spin currents where the location of the barriers vibrate out of phase in time: I_c^x and I_s^x, vs the normalized barriers' chemical potential $\mu_l = \mu_r = \mu$. The parameters are set identical to those

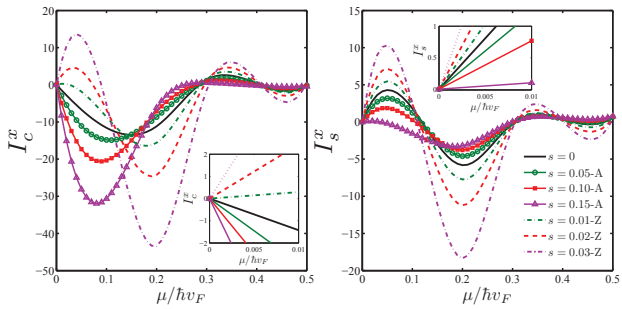

Fig. 3: Adiabatic spin and charge pumping vs $\mu_l = \mu_r = \mu$ where the location of barriers $x_{l,r}$ vibrate around their equilibrium values. The equilibrium location of barriers are set at $x_l = 0$, $x_r = 0.5L$ and the strength of ESCOs fixed at $\alpha_l = \alpha_r = 3.5\hbar v_F$. $s = 0.05, 0.10, 0.15$ and $s = 0.01, 0.02, 0.03$ are values considered for the strength of A- and Z strains applied to the device, respectively.

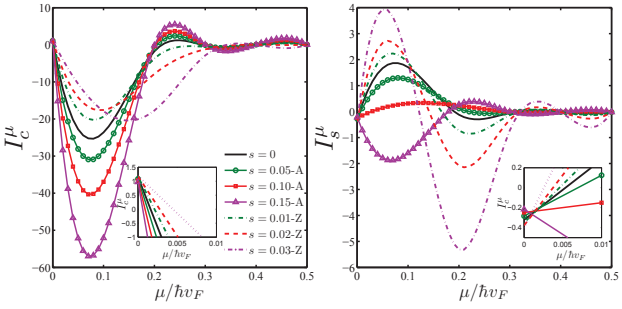

Fig. 4: Adiabatically pumped charge and spin currents where the chemical potentials $\mu_{l,r}$ at the barriers vibrate around their equilibrium values: I_c^μ and I_s^μ. The locations and ESOCs of the barriers are assumed fixed at $x_l = 0$, $x_r = 0.5L$, and $\alpha_l = \alpha_r = 3.5\hbar v_F$, respectively. The strength of strain applied to the device is equal to $s = 0.05, 0.10, 0.15$ in the A-strain and $s = 0.01, 0.02, 0.03$ in the Z-strain classes.

of Fig. 2. Here, the pumped charge and spin currents have the same order of magnitudes, but they are at least three orders of magnitude greater than the pumping through time dependent ESOCs at the barriers (see Figs. 2 and 3). Unlike the pumped currents generated by oscillating ESOCs where strain has similar effects on the spin and charge currents, the increment of strain strength in the A-direction here induces an overall enhancement in the pumped charge current while it causes an overall suppression in the spin current. However, the increment of strain strength in Z-direction has similar effects on the pumped spin and charge currents and causes overall enhancement in both the spin and charge currents. Similar to Fig. 2, we see that the charge and spin currents are zero at $\mu_l = \mu_r = 0$ which is clearly apparent in the inset panels. We now turn to the most important operation mode, namely where the pumping parameters are the chemical potentials at the barriers $\mu_{l,r}$, oscillating adiabatically around their equilibrium values. Results are shown in Fig. 4 and all of the parameters are set at identical values to the two previous cases. We find that the amplitudes of the pumped currents have the same order of magnitudes as Fig. 3 where the location of barriers vibrate around their equilibrium values. As in the previous cases, strain has pronounce influences on the pumped charge and spin currents. Further investigations demonstrate that increasing the strain strength in the A-direction increases the overall amplitude of the pumped charge current, but decreases the overall amplitude of the spin current. On the other hand, the increment of the Z-strain has opposite effects on the spin and charge currents. These unequal effects of the strain on the pumped charge and spin currents offers an experimentally feasible fashion to manipulate and control pumping of the charge and spin currents through the device. The inset panels illustrate the behavior of charge and spin currents near $\mu_{l,r} \sim 0$. In contrast to the previous cases, we see that the charge and spin currents are nonzero at $\mu_{l,r} = 0$. The absence of threshold value in chemical potential to generate the currents and nonzero value of the current pumped in Fig. 4 result from the linear dispersion relation and chiral nature of Fermions in grphene [18, 23]. In effect, our further investigations demonstrate that to generate and manipulate the spin current, the chemical potential should be '*nonzero*'. This is shown by the inset panels of Figs. 2 and 3 where no spin current passes through the system at the zero chemical potential $\mu = 0$. This issue however disappears where the chemical potentials oscillate around an equilibrium value even at $\mu = 0$. Hence, by considering the amplitudes of adiabatically pumped currents ($I_{c,s}^\alpha$, $I_{c,s}^x$, $I_{c,s}^\mu$) and the manipulation of spin currents over a wide range of $\mu_{l,r}$, one concludes that oscillating chemical potentials at the barriers would provide more effective mechanism to generate spin current and control the magnitude of charge and spin currents through strain.

In conclusion, we have proposed a novel quantum pump consisting of a strained graphene monolayer with intrinsic spin-orbit coupling and two vibrating extrinsic spin-orbit coupled barriers. To generate adiabatically pumped currents we consider three different operation modes to the device: i) the strength of extrinsic spin-orbit couplings, ii) the locations and ii) the chemical potential of the barriers oscillate out of phase in time. We have shown that such a device operates with largest amplitude of pumped currents where the chemical potential of the barriers oscillates in time and drives the charge and spin currents into the system. Our results have found that this operation mode has also broader functionality range in terms of parameters compared with the other modes. Our study revealed that a strain applied to the plane of graphene layer can play key roles to control and manipulate the spin and charge currents separately, namely one can tune the spin current and suppress the charge current simultaneously. This interesting phenomenon originates from the opposite effects of strain on the pumped spin and charge currents, depending on the direction of strain imposed to the device.

REFERENCES

[1] I. Žutić, J. Fabian and S. D. Sarma, Rev. Mod. Phys. **76**, 323 (2004).
[2] S. K. Novoselov, et. al., Science **306**, 666 (2004).

[3] Y. Zhang, W. Y. Tan, L. H. Stormer and P. Kim, Nature, **438**, 201 (2005).
[4] H. A. Castro Neto, F. Guinea, R. M. N. Peres, S. K. Novoselov and K. A. Geim, Rev. Mod. Phys., **81**, 109 (2009).
[5] Kh. Shakouri, M. Ramezani Masir, A. Jellal, E. B. Choubabi, and F. M. Peeters, Phys. Rev. B **88**, 115408 (2013); V. Szaszk-Bogr, F. M. Peeters, P. Fldi, Phys. Rev. B **91**, 235311 (2015).
[6] K. Hasanirokh, J. Azizi, A. Phirouznia, H. Mohammadpour, Eur. Phys. J. B **87**, 95 (2014).
[7] W. Han, Roland K. Kawakami, M. Gmitra and J. Fabian, Nat. Nanotech., **9**, 794 (2014).
[8] A. Avsar, et. al. Nat. Comm., **5**, 4875 (2014).
[9] C. L. Kane and E. J. Mele, Phys. Rev. Lett. **95**, 226801 (2005).
[10] D. Marchenko, A. Varykhalov, M. R. Scholz, G. Bihlmayer, E. I. Rashba, A. Rybkin, A. M. Shikin, and O. Rader, Nature Commun. **3**, 1232 (2012).
[11] A. Dyrdal, J. Barnaś, and V. K. Dugaev, Phys. Rev. B **89**, 075422 (2014).
[12] D. Bercioux, F. D. Urban, F. Romeo, and R. Citro, Appl. Phys. Lett. **101** 122405 (2012).
[13] M. M. Grujić, M. Z. Tadić and F. M. Peeters, Phys. Rev. Lett. **113**, 046601 (2014).
[14] Y. Yao, F. Ye, X. Qi, S. Zhang, and Z. Fang, Phys. Rev. B **75**, 041401(R) (2007).
[15] F. Zhai, Y. Ma and K. Chang, New J. Phys. **13** 083029 (2011).
[16] Yu. Makhlin, and A. D. Mirlin, Phys. Rev. Lett. **87** 276803 (2001); F. Zhou, B. Spivak and B. Altshuler, Phys. Rev. Lett. **82** 608 (1999).
[17] P. W. Brouwer, Phys. Rev. B **58**, R10135 (1998); M. Moskalets, M. Buttiker, Phys. Rev. B **66**, 035306 (2002).
[18] E. Prada, P. San-Jose and H. Schomerus, Phys. Rev. B **80**, 245414 (2009); E. Prada, P. SanJose and H. Schomerus, Solid State Commun **151**, 1065 (2011).
[19] E. Grichuk and E. Manykin, Eur. Phys. J. B **86**, 210 (2013).
[20] C. Benjamin, Appl. Phys. Lett. **103**, 043120 (2013).
[21] R. Zhu and H. Chen Appl. Phys. Lett. **95** 122111 (2009).
[22] T. Low, Y. Jiang, M. Katsnelson and F. Guinea, Nano Lett. **12**, 850 (2012).
[23] B. Abdollahipour and R. Mohammadkhani, J. Phys.: Condens. Matter, **26**, 085304 (2014).
[24] Q. Zhang, K. S. Chan, Z. Lin, Appl. Phys. Lett. **98**, 032106 (2011); Q. Zhang, K. S. Chan, Z. Lin, J. Liu, Phys. Lett. A **377**, 632 (2013); J. Wang, K. S. Chan, and Z. Lin, Appl. Phys. Lett. **104**, 013105 (2014).
[25] A. Kundu, S. Rao, and A. Saha, Phys. Rev. B **82**, 155441 (2010).
[26] S. Singh , A. K. Patra , B. Barin , E. del Barco , and B. Ozyilmaz, EEE Trans. Mag. **49**, 3147 (2013).
[27] J. Balakrishnan, G. K. W. Koon, M. Jaiswal, A. H. Castro Neto and B. Ozyilmaz, Nat. Phys. 9, 284287 (2013).
[28] V. M. Pereira, A. H. Castro Neto and N. M. R. Peres, Phys. Rev. B **80**, 045401 (2009).
[29] S.-M. Choi, S.-H. Jhi and Y.-W. Son, Phys. Rev. B **81**, 081407(R) (2010).
[30] B. Soodchomshom, Physica B **406**, 614 (2011); B. Soodchomshom, J. Supercond. Nov. Magn. 24, 1715 (2011).
[31] F. Liu, P. Ming, and J. Li, Phys. Rev. B **76**, 064120 (2007).
[32] C. Lee, X. Wei, J. W. Kysar, J. Hone, Science 321, 385 (2008).
[33] M. Titov, Europhys. Lett. **79**, 17004 (2007).
[34] M. Alidoust, and J. Linder, Phys. Rev. B **84**, 035407 (2011).
[35] L. Covaci and F. M. Peeters, Phys. Rev. B **84**, 241401(R) (2011).